| Title | Graphene-Based FET Detector for E. coli K12 Real-Time Monitoring and Its Theoretical Analysis |
| --- | --- |
| Author(s) | ZHU, J; NIU, F; ZHU, C; YANG, J; Xi, N |
| Citation | Journal of Sensors, 2016, v. 2016, p. 4641398:1-9 |
| Issued Date | 2016 |
| URL | http://hdl.handle.net/10722/234601 |
| Rights | This work is licensed under a Creative Commons Attribution-NonCommercial-NoDerivatives 4.0 International License. |

*Research Article*

# Graphene-Based FET Detector for *E. coli* K12 Real-Time Monitoring and Its Theoretical Analysis

**Jieyi Zhu,[1,2] Fuzhou Niu,[1,2] Changan Zhu,[1] Jie Yang,[1] and Ning Xi[2]**

[1]*Department of Precision Machinery and Precision Instrumentation, University of Science and Technology of China,*
 *Hefei 230026, China*
[2]*Department of Mechanical and Biomedical Engineering, City University of Hong Kong, Kowloon, Hong Kong*

Correspondence should be addressed to Fuzhou Niu; fzniu@mail.ustc.edu.cn

This paper presents a theoretical analysis for a graphene-based FET real-time detector of the target bacteria *E. coli* K12. The motivation for this study is to design a sensor device for detection of bacteria in food and water in order to guarantee food safety. Graphene is chosen as our material for sensor design, which has outstanding electrical, physical, and optical performance. In our sensor structure, graphene-based solution gate field effect transistor (FET) is the device model; fabrication and functionalization protocol are presented together in this paper. What is more, a real-time signal display system is the accompanied equipment for our designed biosensor device. In this system, the sensor bias current signal $I_{ds}$ would change obviously when the target bacteria are attached to the sensor surface. And the bias current $I_{ds}$ increases when the *E. coli* concentration increases. In the latter part, a theoretical interpretation of the sensor signal is to explain the bias current $I_{ds}$ increasing after the *E. coli* K12 attachment.

## 1. Introduction

Over the last few decades, several kinds of nanostructure biosensors have been designed for industrial and household use. The aim of our study is to realize the detection of bacteria in food and water in order to ensure food security and public health safety. So for this purpose we need to design a micro-nanobiosensor to detect bacteria. The design of nanobiosensors includes the materials and structures. For materials, many semiconductor materials are chosen due to good electrical property and excellent applications in electronic devices. For instance, silicone is often used for biosensor design; an example is the high density microelectrode array biosensor in Radke and Alocilja's paper [1]. For structure, nanostructures include planar, nanowire, nanosphere sensors, even carbon nanotube, and graphene. Graphene is a single layer of carbon atoms which is packed into a hexagonal planar structure. Nowadays, graphene is often chosen as sensing material due to its excellent electrical, physical, and biocompatible properties. Compared to silicon, graphene is a zero-gap semiconductor; it is not easy for electron to scatter in graphene; the carrier mobility of graphene could be as high

as $2 \times 10^5 \, \text{cm}^2/(\text{V·s})$ [2], about 140 times larger than that of silicon [3]. Graphene was discovered in 2004, Novoselov et al. describe graphene as having excellent electrical, optical, and mechanical properties [4]. Thus, graphene becomes a suitable material in electronic applications. During the last two years, many novel graphene-based devices came into being for various kinds of detectors. Specifically, graphene-based sensors could be used in detecting bacteria. Now, our project is to design a biosensor to detect *Escherichia coli*, which is an ordinary bacterium in the issue of food safety. Under this circumstance we develop a graphene-based field effect transistor sensor for detection of *E. coli* bacteria. The spread of *E. coli* bacteria would cause harm to both environment and human body. The pathogenic strain of *E. coli*, like *E. coli* O157:H7, can cause bloody diarrhea, hemorrhagic colitis, and hemolytic uremic syndrome. Compared to the pathogenic strain *E. coli* O157:H7, our target is the nonpathogenic strain *E. coli* K12, which is currently an indicator for laboratory testing. So far, Huang's group has presented a graphene-based FET sensor with functionalization for detection of *E. coli* K12 [5]; their group detects *E. coli*'s concentration and *E. coli*'s metabolic activities. Moreover, the graphene FET
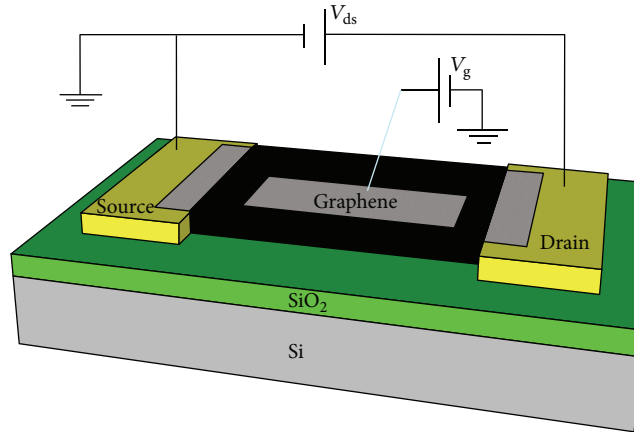
FIGURE 1: The design of solution gate graphene-based field effect transistor. Bias voltage $V_{ds}$ is applied between source and drain electrodes; gate voltage $V_g$ is applied to the solution inside the recording chamber.

device could also be used to detect glucose concentration [6]. Besides, Chang's group uses graphene oxide to realize the biosensor for the target *E. coli* O157:H7. Thermal reduced monolayer graphene oxide was demonstrated to fabricate a graphene oxide-based FET biosensor [7]. However, there is still a limitation that graphene has been shown to have lower sensitivity due to lack of bandgap [8], as the performance of a FET biosensor depends on the subthreshold swing of the device [9]. Compared to Huang's sensor model, our FET model uses Si/SiO$_2$ substrate rather than his quartz substrate. Furthermore, this model could also be applicable to some other 2D materials like TiO$_2$ and MoS$_2$, apart from graphene [10]. This model could be extended to two-dimensional transition metal dichalcogenides (TMDC), because when TMDC is changed into a two-dimensional structure from a block structure, its electrical property will be greatly modified due to its bandgap change [11]. Here, in this paper we will report a graphene-based FET detector together with its fabrication protocol (Figure 2) and functionalization protocol, and its model is a solution gate FET sensor. Then we use the protocol to finish a sensor chip with a recording chamber and test the target bacteria *E. coli* K12's presence and concentration by this chip. In our experiments, we fix our sensor chip on the surface of the probe station, connect the electrical circuit by applying bias voltage and gate voltage through the manipulator of the probe station, and measure the FET bias current by the signal process instrument Keithley 2636B with its real-time recording software. From the measurement, we could get signal response when *E. coli* K12's solution is added onto the sensor's recording chamber. Moreover, *E. coli* K12's solution concentration is changing during the real-time measurement; the relationship between bacteria concentration and bias current $I_{ds}$ would be presented and discussed.

## 2. Biosensor Structure

In our design, the biosensor structure is a graphene-based field effect transistor (FET) sensor. Then this graphene FET is functionalized to be a specific *E. coli* K12 sensor. We choose P doped Si/SiO$_2$ substrate to be the sensor bottom; one side

of the substrate is Si and the other side is SiO$_2$. The thickness of SiO$_2$ layer is 100 nm. Two electrodes are deposited on the SiO$_2$ side of the substrate as source and drain electrodes by metal deposition. Graphene nanoribbon (1.1 mm × 0.6 mm) is placed across these two electrodes according to a graphene transfer protocol. Besides, silicone rubber is used to coat around the graphene to form a recording chamber. The bias voltage $V_{ds}$ is applied between source and drain electrodes, letting the two manipulator needles touch the source and drain electrodes. Usually, there are two kinds of FET, back-gate FET and solution gate FET. For our real-time measurement we choose solution gate FET. The gate voltage $V_g$ is applied by inserting the third manipulator needle immersed into the solution inside the recording chamber. The source-drain bias and source-gate bias share a common ground, avoiding significant fluctuations in the gate voltage actually applied on graphene. In actual experiments we use wires to connect the source electrode to the probe station for ground connection. The schematic diagram of our biosensor design is shown in Figure 1.

## 3. Fabrication and Functionalization

*3.1. Fabrication of Microchip.* In order to realize the designed microchip, we need to finish device fabrication. The first process is the fabrication of substrate with electrodes. Clean the Si/SiO$_2$ substrate in acetone, alcohol, IPA, and DI water for 10 min in plasma cleaner and spin-coat photoresist on the SiO$_2$ side surface of the substrate. Then prebake the die on hot plate at 110°C for 10 min. After that a photolithography process is done with a designed photomask for the electrodes pattern. Two electrodes (source and drain) are deposited on the Si/SiO$_2$ substrate by two layers of metal deposition, 15 nm Cr and 100 nm Au, by the instrument Q150 TS. After that, photoresist on the substrate is washed away by acetone. The second process is graphene direct transfer process. A layer of PMMA is coated on the copper of graphene/Cu sheet; wait around half an hour for drying off. Put the PMMA/graphene/Cu sheet into FeCl$_3$ aqueous solution at room temperature for Cu layer etching and wait for about
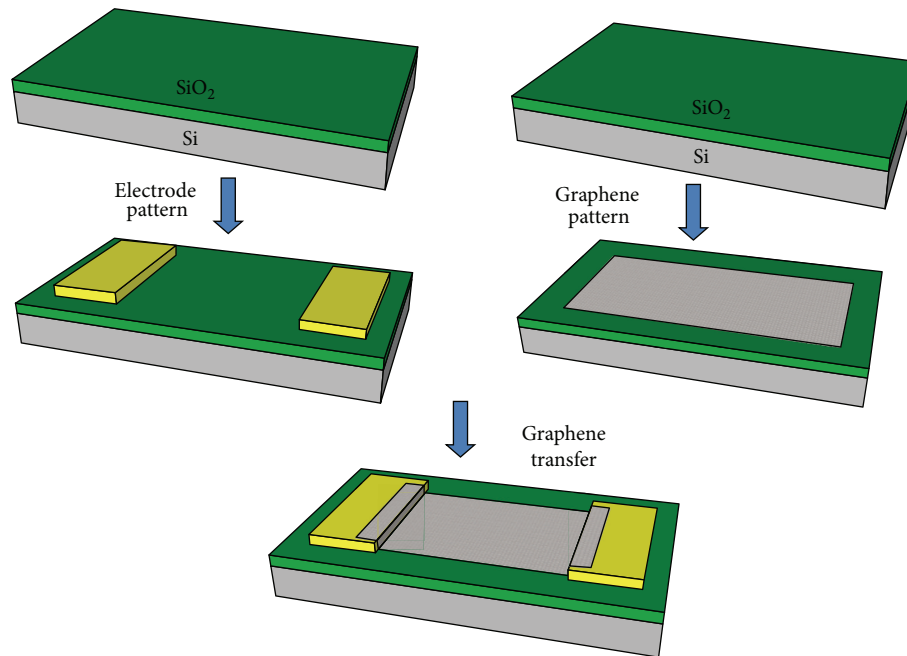
FIGURE 2: The illustration of fabrication protocol for our microchip. Electrode pattern and graphene pattern are finished in two photolithography processes.

10 hours; the PMMA/graphene layer would detach from PMMA/graphene/Cu sheet. The PMMA/graphene layer is picked up by using a pair of tweezers with a spare substrate. Wash and rinse with DI water three times to remove Fe and Cu ions; three petri dishes with DI water are prepared for this step. At last, put the PMMA/graphene layer on the Si/SiO$_2$ substrate, and use tissue to sip up moisture on the surface of this die. Bake this die with PMMA/graphene layer at 80°C for 5 min first, and then bake it at 150°C for 15 min. After the baking, drip one drop of PMMA onto the surface of each die. Lastly, acetone is used to wash away the PMMA layer. The third process is another photolithography for graphene pattern and graphene transfer to the electrodes. Take one die already with graphene after the second process and design a photomask for graphene pattern. After that, put this die under microscope, choose one appropriate graphene nanoribbon, and mark this one on the platform of probe station. Drip PMMA onto the chosen area, observing it under microscope to make the chosen nanoribbon be covered by PMMA. After 10 minutes, pick out the die by tweezers, and put this die immersed into a Petri dish of DI water. With needle and other tools' help, the graphene layer is picked up and put onto the substrate with electrodes. Then the graphene layer is adjusted to fit with the substrate, letting the chosen graphene nanoribbon across the two electrodes form an electrical circuit. The adjustment is done by manipulation of probe station.

*3.2. Functionalization of the Biomolecules.* After device fabrication, the graphene-based FET sensor needs to be functionalized. Firstly, a solution of 6 mM 1-pyrenebutanoic acid succinimidyl ester (1-PBSE) in dimethylformamide (DMF) is prepared. Then the device is incubated with this 6 mM 1-PBSE (Sigma-Aldrich, 457078) dimethylformamide (DMF, Sigma-Aldrich, D4551) solution for 2 h at room temperature. Then the sensor chip is thoroughly rinsed in DMF to wash away the excess reagent. Secondly, the antibody incubation of the chip, a 50 ppm anti-*E. coli* O + *E. coli* K antibody (Abcam 33604) in DI water solution, is prepared. During this step the sensor device is incubated overnight (about 16–18 hours) in this 50 ppm anti-*E. coli* O&K FITC antibody (Abcam 33604) solution at 4°C. Thirdly, the microchip is incubated with 0.1 M ethanolamine (pH 9.0) for 1 h. Fourthly, the device is incubated with 0.1% Tween 20. The whole process of functionalization is shown in Figure 3. After all, the silicone rubber (Dow Corning) is coated around the graphene nanoribbon to form a recording chamber.

## 4. Experiment and Real-Time Data

*4.1. Experiment and Real-Time Data.* In our experiment, when we finish both fabrication and functionalization, we place the chip on the surface of our probe station. The chip is fixed on the probe station platform by magnetic force. The two manipulator needles contact source and drain electrodes, providing bias voltage from Sourcemeter Keithley 2636B. The third manipulator needle contacts the solution inside the recording chamber, providing gate voltage. The schematic diagram of the sensor structure is shown in Figure 1. During our measurement, we add PBS and *E. coli* solution into the recording chamber of the sensor. Usually, there are two kinds of FET, back-gate FET and solution gate FET. In our experiment we choose solution gate FET for the real-time measurement, and the schematic diagram of solution gate FET is shown in Figure 4.
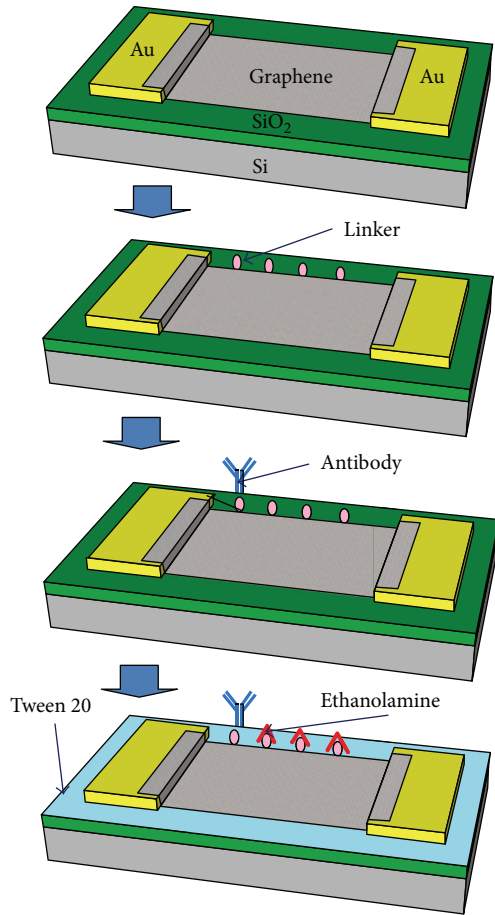
FIGURE 3: The schematic diagram of functionalization process for our biosensor surface. Our chosen linker is 1-pyrenebutanoic acid succinimidyl ester; the antibody is anti-*E. coli* O&K antibody (Abcam 33604).

The data acquisition system includes the Sourcemeter Keithley 2636B and its real-time signal recording program. After the experimental setup is finished, we turn on the Sourcemeter Keithley 2636B and initialize the real-time signal recording program. Besides, we need to culture the bacteria *E. coli* K12 before the real-time measurements. *E. coli* K12 ER2925 is purchased from Eastwin International Trading Limited, Hong Kong. We culture the bacteria in Luria Bertani (LB) medium overnight at 37°C. The bacteria solution after overnight culture is the next passage. The original *E. coli* K12 bacteria solution is passaged to the third generation before the experimental week. Before the measurement, the bacteria are passaged to the fourth generation or the fifth generation. In our real-time measurement, we use the fifth generation of the bacteria. In order to calculate the concentration of the experimental *E. coli* solution, we use colony counting method. The fifth-generation bacteria solution is determined to be $2 \times 10^8$ CFU/mL. The stock is diluted in PBS solution (pH 7.2) 10 times to produce the desired final concentration of *E. coli* K12 for experiments, $2 \times 10^7$ CFU/mL. The dilution is conducted in a minicentrifuge tube with 1 mL of PBS and 100 $\mu$L of the fifth-generation bacteria solution. At last, we
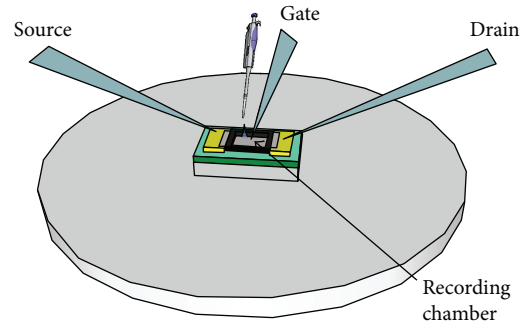


FIGURE 4: The schematic diagram of graphene-based solution gate FET experimental setup on our probe station. The circle plate stands for the probe station plate; the three blue needles stand for the manipulator needles.

start our real-time bias current recording; firstly 5 $\mu$L of PBS is added into the recording chamber, and then add 30 $\mu$L *E. coli* experimental solution 6 times (5 $\mu$L each time). In the last three times of addition, we find bias current signal change. Theoretically, the sensor should have signal once we add bacteria solution; however the mixture of solution needs some time, so it is acceptable that there is time delay during the first four times of solution addition. And the change of gate electrode immersion length would lead to some errors in our measurement. During our experiment, we keep gate voltage $V_g = 0$ V and bias voltage $V_{ds} = 0.1$ V. The real-time figure is shown in Figure 5.

Summarily, there are six times of *E. coli* K12 solution addition along the real-time measurement. Each time the addition amount is 5 $\mu$L. During the first three addition times, there are not apparent signal changes and the bias current $I_{ds}$ is around 7 $\mu$A. After the fourth addition, the bias current $I_{ds}$ increases from 7 $\mu$A to 7.5 $\mu$A before the next addition. The fifth addition time is corresponding to 0 s in the real-time figure. After the fifth addition, the bias current $I_{ds}$ increases from 7.5 $\mu$A to 9 $\mu$A before the sixth addition. The sixth addition time is corresponding to 30 s in the real-time figure. After the sixth addition, the bias current $I_{ds}$ increases from 9 $\mu$A to 9.7 $\mu$A.

*4.2. Characterization.* After our experiment, we conduct the characterization of our experimental sensor chip by atomic force microscopy (AFM) scanning. The AFM image shows the graphene nanoribbon across the two electrodes. And we scanned the experimental sensor chip after *E. coli* attachment in tapping mode. The AFM we recorded is shown in Figure 6.

## 5. Theoretical Analysis

After we acquired the bias current $I_{ds}$, we started to analyze and explain the experimental results by our theoretical derivation and simulation. Consider that our sensor model is a planar FET sensor, and the sensor surface is functionalized with specific receptors, which is the linker-antibody for the target *E. coli* K12 bacteria molecules. So the conjugation calculation is based on the Langmuir adsorption equation.
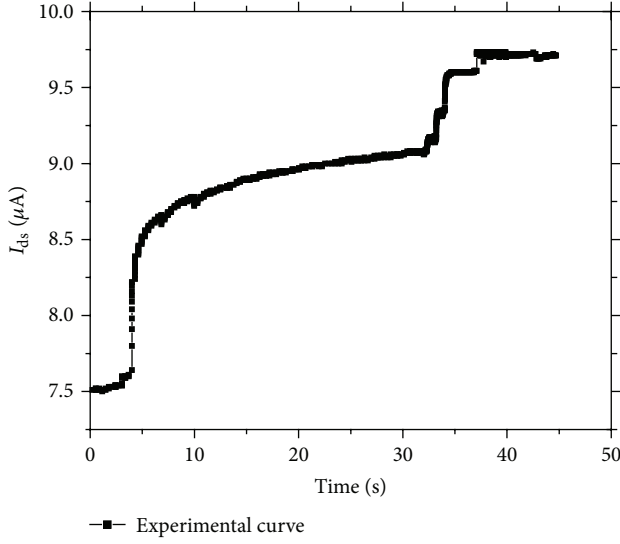
FIGURE 5: The real-time bias current $I_{ds}$ signal curve during our measurement.
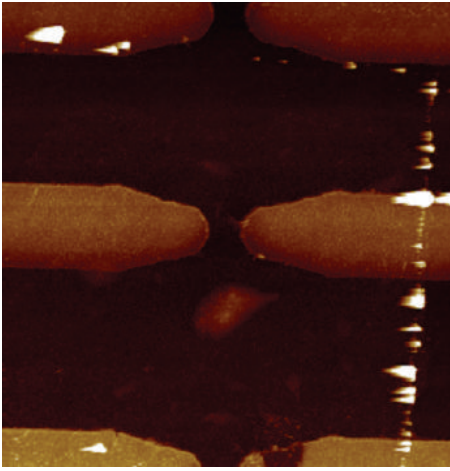


FIGURE 6: AFM image of the sensor chip after experimental process.

And firstly the adsorption model is regarded as an ideal model without doping effect. If we set the initial addition time as $t = 0$ s, the conjugation rate between the target bacteria E. coli K12 molecules and the receptors is given by the following equation [12]:

$$\frac{dN}{dt} = k_F (N_0 - N) \rho_0 - k_R N. \tag{1}$$

In this equation, $N$ is the density of conjugated receptors, $N_0$ is the receptors' density when $t = 0$ s, $k_F$ and $k_R$ are adsorption constant and desorption constant between target molecules and the linker-antibody receptors, and $\rho_0$ is the concentration of the analyte target. The conjugation number increases from the start time $t = 0$; at one time the conjugation number becomes steady until the next addition. The Langmuir parameters are acquired from the adsorption

isotherm experiment. The equation of conjugation numbers is given by a group of equations as follows [13]:

$$N(t) = \rho_0 t \left( \frac{\sqrt{2Dt}}{D} + \frac{1}{k_F N_0} \right)^{-1},$$

$$N_T(t \to \infty) = \frac{k_F N_0 \rho_0}{k_F \rho_0 + k_R} = \frac{k_T N_0 \rho_0}{k_T \rho_0 + 1}. \tag{2}$$

In this group of equations, $N(t)$ is the conjugation numbers before equilibrium and $N_T(t \to \infty)$ is the conjugation numbers after equilibrium. The equilibrium condition stands for the fact that that the conjugation numbers become saturate. $D$ is the diffusion coefficient. The normalized Langmuir parameter $k_T$ is calculated as $k_T = k_F/k_R$, and $\rho_0$ is the concentration of the analyte target. For the two signal steps, the first one is corresponding to the fifth addition; after the fifth addition the target concentration is $1.67 \times 10^7$ CFU/mL. The second one is corresponding to the sixth addition; after the sixth addition the target concentration is $1.7 \times 10^7$ CFU/mL. According to the I-V curve equation, the carrier density is calculated as $n = I_{ds} L/(WV_{ds} q \mu_{eff})$. $V_{ds} = 0.1$ V, $e = 1.6 \times 10^{19}$ C, $\mu_{eff} = 1200$ cm$^2$/V·s, $W/L = 60/110$. Thus, the carrier density figure along the real-time signal measurement is shown in Figure 7.

In the carrier density real-time Figure 7, we could find the corresponding relationship between bacteria concentration and carrier density. After calculating from the full real-time data, we could find that the carrier density before bacteria attachment is $6.68 \times 10^{11}$/cm$^2$. Then the relationship between bacteria concentration and carrier density is listed in Table 1.

The two groups of simulation parameters are below. The Langmuir parameter is $k_T = k_F/k_R = 5.88 \times 10^6$/mol [14], the target molecule size is $2\,\mu$m, the oxidation thickness is $100\,\mu$m, and the diffusion coefficient $D$ is $7.6 \times 10^6$. The target concentration for the fifth addition is $1.67 \times 10^7$ CFU/mL, and the target concentration for the sixth addition is $1.7 \times 10^7$ CFU/mL. From the MATLAB calculation of (2), a simulation curve is acquired based on the target-receptor adsorption model. The simulation curve is shown in Figure 8.

The above carrier density calculation is based on an ideal condition without doping. In fact, carrier density depends on multiple factors such as doping level. The graphene we used in our experiment is the copper-based CVD graphene. Even under the circumstance of $V_g = 0$, the copper-based CVD graphene is usually already P doped. And the doping level could be tuned by gate voltage via field effect. We could find difference between experimental curve and calculation curve. In this case, we could use the difference of gate voltage and Dirac voltage to reflect the doping level caused by applied gate voltage. According to the reference considering the effects of doping level [15], the equation of carrier density calculation would be modified as shown in (3); $C_g$ and $V_0$ stand for gate capacitance and Dirac voltage, respectively. Consider

$$n = \sqrt{n_0^2 + \left( \frac{C_{ox}(V_g - V_D)}{e} \right)^2}. \tag{3}$$

Table 1: The relationship between bacteria concentration and carrier density.

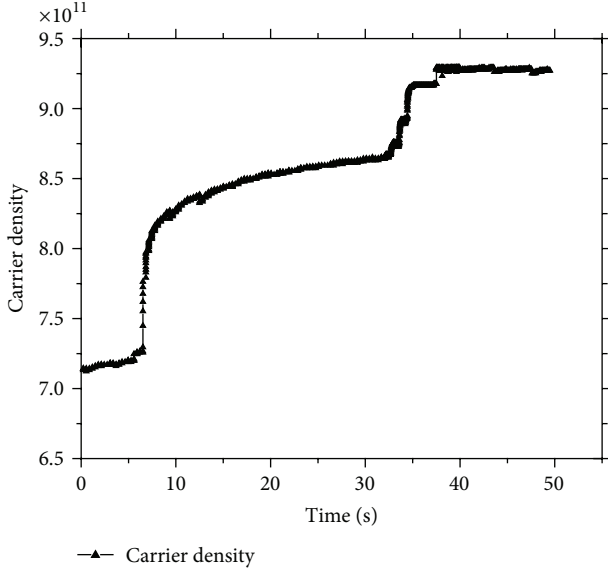| E. coli K12 concentration (CFU/mL) | 0 | $1.6 \times 10^7$ | $1.6 \times 10^7$ | $1.7 \times 10^7$ |
|---|---|---|---|---|
| Carrier density (/cm$^2$) | $6.68 \times 10^{11}$ | $7.1 \times 10^{11}$ | $8.5 \times 10^{11}$ | $9.26 \times 10^{11}$ |



Figure 7: The graphene channel's carrier density along the real-time sensor signal measurement.

Next we will analyze the electrical property of our material graphene. Graphene is made out of carbon atoms arranged in hexagonal structure. Intrinsic graphene is a zero-gap semiconductor [16]; in order to calculate the energy bands of graphene, we could deduce that from tight-binding model. After a series of calculation of vectors and Hamiltonian, the energy bands equation is as follows [17]:

$$E_{\pm}(k) = \pm\sqrt{3 + f(k)} - t'f(k), \tag{4}$$

$$f(k) = 2\cos\left(\sqrt{3}k_y a\right) + 4\cos\left(\frac{\sqrt{3}}{2}k_y a\right)\cos\left(\frac{3}{2}k_x a\right). \tag{5}$$

In these two equations, $t(\approx 2.8\,\text{eV})$ is the nearest-neighbor hopping energy (hopping between different sublattices) and $f(k)$ is wave function in the graphene plane. $k_x$ and $k_y$ are horizontal vector and vertical vector and $a$ is the distance between two neighbor carbon atoms, $a \approx 1.42\,\text{A}$. Combining (4) and (5) together, we could get the energy band equation as follows [18]:

$$E_{\pm}(k) = \pm 2.8\sqrt{3 + 2\cos\left(\sqrt{3}k_y a\right) + 4\cos\left(\frac{\sqrt{3}}{2}k_y a\right)\cos\left(\frac{3}{2}k_x a\right)}. \tag{6}$$


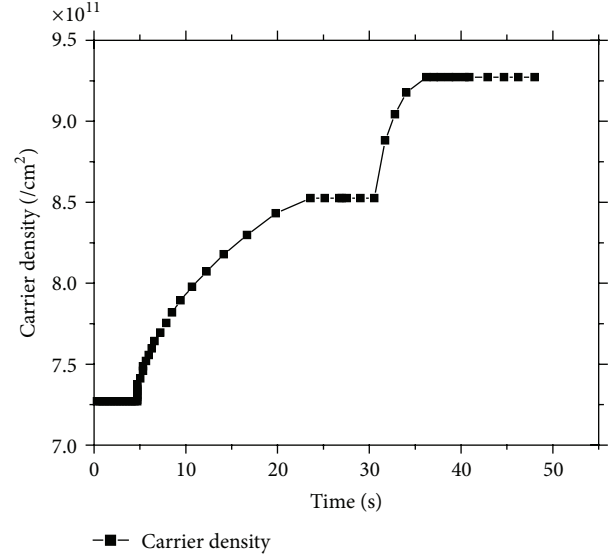
Figure 8: Simulation figure for the two responses due to our fifth addition and the sixth addition of E. coli K12 solution.
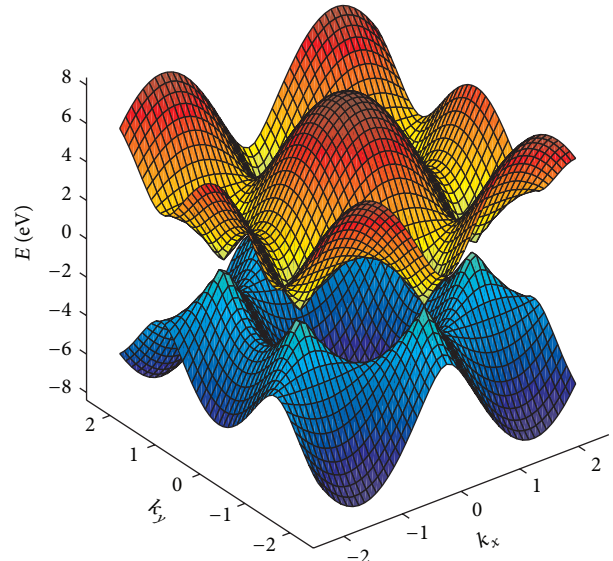


Figure 9: The simulation figure of graphene energy band structure. The upper curve stands for the conduction band and the lower curve stands for the valence band.

From this equation, we could draw out the graphene's energy band by MATLAB. After inputting a MATLAB calculation program, we could draw out a three-dimensional energy band structure, as shown in Figure 9.

For intrinsic graphene, the conduction band and the valence band contact at one point, which is called Dirac point, and Fermi energy band is across the Dirac point. When it is for P doping graphene or N doping graphene, graphene's Fermi surface would shift down or move up. In our experiment, the target bacteria E. coli K12 carry negative charge on their molecule; when E. coli K12 molecules are adsorbed onto the functionalized surface of graphene, they

will induce positive charge in the graphene channel, causing more holes and leading holes to become majority carriers. Thus, our *E. coli* K12 real-time experiment is a P doping example. However, it is difficult to precisely measure the doping level caused by *E. coli* attachment, as the graphene is already P doped before *E. coli* attachment. The difference between intrinsic graphene and P doping graphene is shown in Figure 10.

In our real-time measurement, we use the bias current $I_{ds}$ as the electrical signal. For graphene FET sensors, usually there are two important curves: *I-V* curves and transfer curves. *I-V* curves present the relationship between bias current $I_{ds}$ and bias voltage $V_D$ when gate voltage $V_g = 0$ V. Transfer curves present the relationship between bias current $I_{ds}$ and gate voltage $V_g$ with a fixed bias voltage $V_D$. In our real-time measurement, we always set the gate voltage $V_g = 0$ V. The current-voltage relationship is deduced from the Landauer formula [19], which can define the conductance equation of the monolayer graphene model. In the Landauer formula, $e$ is the electron charge, $h$ is Planck's constant, and $f(E)$ is the probability of the Fermi level with electrons, which is known as the Fermi-Dirac distribution function. Consider

$$G = \frac{2e^2}{h} \int_0^{+\infty} M(E) T(E) \left( -\frac{df(E)}{dE} \right) dE. \tag{7}$$

Then in Meric's GFET electrical model, he deduced the current-voltage equation from the basic Landauer formula, considering the drift velocity $v_{drift}$ and carrier density $n$. Consider

$$I_d = \frac{W}{L} \int_0^L en(x) v_{drift}(x) dx. \tag{8}$$

In Meric's paper, the author raises a compact model for graphene FET [20]. Besides, Parrish's paper also provides reference for a compact model of graphene FET [21]. Combining these references together, we could acquire a group of equations for both *I-V* curves and transfer curves. Consider

$$I_{ds} = e \frac{W}{L} \mu_{eff} n_0 V_{ds} \tag{9}$$

$$I_{ds} = \frac{(W/2L) e\mu_{eff} \left( -C_{ox} \left( V_g - V_D \right) /e + \sqrt{n_0^2 + \left( C_{ox} \left( V_g - V_D \right) /e \right)^2} \right) V_{ds}}{1 + \mu_{eff} V_{ds}/L v_{sat}}. \tag{10}$$

After *E. coli* attachment, we would consider the induced charge caused by the attached *E. coli* molecules. In this case, the current equation would be modified in

$$I'_{ds} = e \frac{W}{L} \mu_{eff} \left( n_0 + \frac{V_I}{V_T} \cdot c \cdot \frac{\rho_0 k_T}{\rho_0 k_T + 1} \cdot Q_E \right) V_{ds} + \Delta I_d. \tag{11}$$

In these equations, (9) and (11) describe graphene FET *I-V* curve characteristic when gate voltage $V_g = 0$ V before *E. coli* attachment and after *E. coli* attachment and (10) describes graphene FET transfer curve characteristic with a fixed bias voltage. For these parameters, $W$ and $L$ are the graphene channel width and length, $\mu_{eff}$ is the effective carrier mobility in graphene channel, $n_0$ is the initial carrier density without gate voltage, $V_g$ is gate voltage, $V_D$ is threshold voltage at Dirac point, $V_{ds}$ is bias voltage, $C_{ox}$ is the oxidation layer gate capacitance, $v_{sat}$ is saturation velocity, $V_I$ and $V_T$ are the injection volume and total volume, respectively, $c$ is the *E. coli* concentration, $Q_E$ is the charge quantity each *E. coli* molecule carries, and $\Delta I_d$ is current change caused by *E. coli* doping.

According to the transfer curves equation, the simulated transfer curves are finished to compare intrinsic graphene and P doping graphene transfer characteristics. The P doping transfer curve is a schematic curve, not in very precise calculation. Thus, in the simulation (Figure 11), we could see that in P doping circumstance, the transfer curve right shifts. The bias current $I_{ds}$ value at $V_g = 0$ increases after P doping. So it can explain why, after *E. coli* attachment, the real-time bias current signal increases. For parameters $e = 1.6 \times 10^{19}$ C,

the graphene width and length are $W = 0.6$ mm and $L = 1.1$ mm, carrier mobility is $\mu_{eff} = 1200$ cm$^2$/V·s, the intrinsic carrier density is $n_0 = 6.68 \times 10^{11}$/cm$^2$, the oxidation gate capacitance is $C_{ox} = 400$ nF [22], and the saturation velocity $v_{sat}$ is $v_{sat} = 5.5 \times 10^6$ cm/s according to one reference paper [23]. The data fitting of *I-V* curves corresponding to three *E. coli* K12 concentrations are in Figure 12.

Above all, we compare three data fitting *I-V* curves according to the real-time measurement. In our data fitting curves (Figure 12), the blue curve is corresponding to the 0 s in the real-time figure (Figure 5), which is after the fourth addition, and the *E. coli* K12 concentration is $1.6 \times 10^7$ CFU/mL. The purple curve is corresponding to the 25 s in the real-time figure (Figure 5), which is after the fifth addition, and the *E. coli* K12 concentration is $1.67 \times 10^7$ CFU/mL. The deep blue curve is corresponding to the 40 s in the real-time figure (Figure 5), which is after the sixth addition, and the *E. coli* K12 concentration is $1.7 \times 10^7$ CFU/mL.

## 6. Conclusion

In summary, we have developed a graphene FET detector for the target *E. coli* K12 and recorded real-time bias current $I_{ds}$ signal measurement; then a theoretical study is conducted to explain the signal. In our analysis, we explained that after the *E. coli* K12 molecules with negative charge attach on the sensor surface, the bacteria will induce holes increasing in
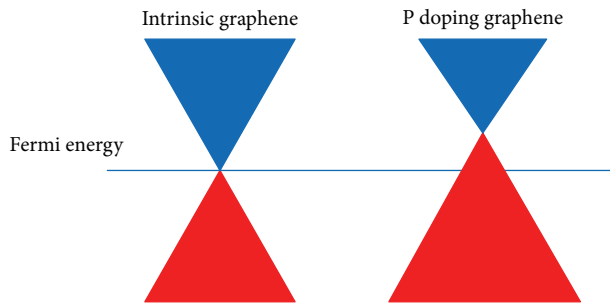
Figure 10: The comparison between intrinsic graphene energy band and P doped graphene energy band. The left figure stands for the intrinsic graphene energy band and the right figure stands for the P doped graphene energy band.
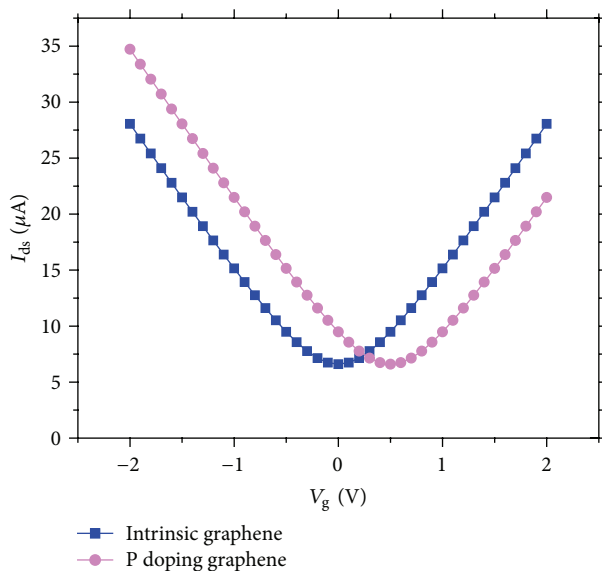


Figure 11: The qualitative transfer curves of intrinsic graphene FET and P doped graphene FET.



Figure 12: Data fitting of $I$-$V$ curves corresponding to three $E.\ coli$ K12 concentrations.

## Authors' Contributions

Jieyi Zhu and Fuzhou Niu contributed equally to this work.

## Acknowledgments

## References

[1] S. M. Radke and E. C. Alocilja, "A high density microelectrode array biosensor for detection of *E. coli* O157:H7," *Biosensors and Bioelectronics*, vol. 20, no. 8, pp. 1662–1667, 2005.

[2] K. I. Bolotin, K. J. Sikes, Z. Jiang et al., "Ultrahigh electron mobility in suspended graphene," *Solid State Communications*, vol. 146, no. 9-10, pp. 351–355, 2008.

[3] K. S. Kim, Y. Zhao, H. Jang et al., "Large-scale pattern growth of graphene films for stretchable transparent electrodes," *Nature*, vol. 457, no. 7230, pp. 706–710, 2009.

[4] K. S. Novoselov, A. K. Geim, S. V. Morozov et al., "Electric field effect in atomically thin carbon films," *Science*, vol. 306, no. 5696, pp. 666–669, 2004.

[5] Y. Huang, X. Dong, Y. Liu, L.-J. Li, and P. Chen, "Graphene-based biosensors for detection of bacteria and their metabolic activities," *Journal of Materials Chemistry*, vol. 21, no. 33, pp. 12358–12362, 2011.

[6] Y. Huang, X. Dong, Y. Shi, C. M. Li, L.-J. Lai, and C. Peng, "Nanoelectronic biosensors based on CVD grown graphene," *Nanoscale*, vol. 2, no. 8, pp. 1485–1488, 2010.

the graphene channel. Thus, the bias current of graphene FET increases due to the carrier numbers increasing. A calculation based on target-receptor model is conducted to be compared with the experimental result. Finally, a simulation based on $I$-$V$ curve equation and data fitting is done to present the relationship of the bias current $I_{ds}$ and the $E.\ coli$ K12 concentration. The real-time measurement result indicates that our sensor chip could have a proportional relationship between bias current $I_{ds}$ signal response and different bacteria concentrations. Thus, our sensor chip has application value for detecting the presence and concentration of $E.\ coli$ K12. Moreover, in future, this biosensor may be modified for detecting the pathogenic strain $E.\ coli$ O157:H7, becoming more useful in ensuring food or environmental safety.

## Competing Interests

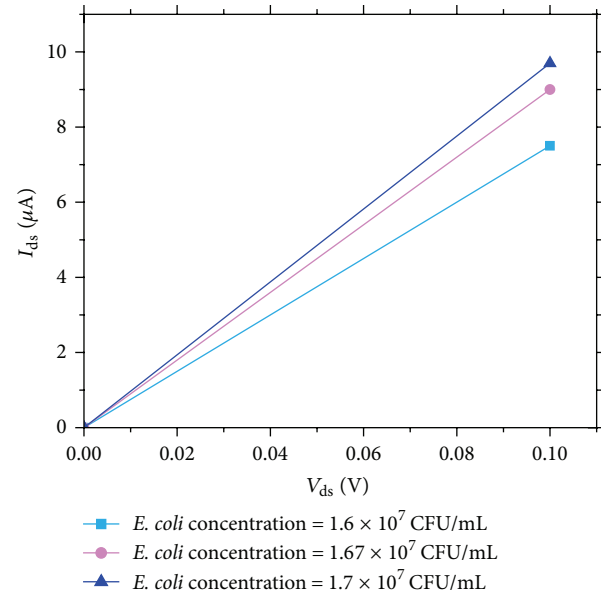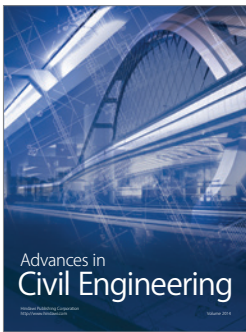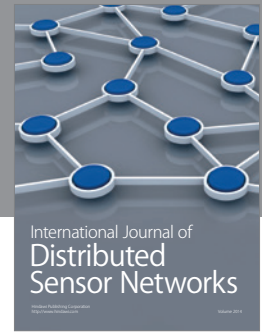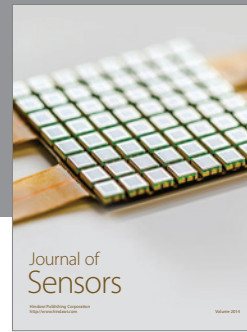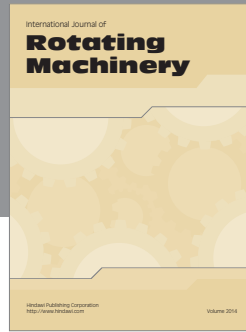The authors declare that they have no competing interests.

[7] J. Chang, S. Mao, Y. Zhang et al., "Ultrasonic-assisted self-assembly of monolayer graphene oxide for rapid detection of *Escherichia coli* bacteria," *Nanoscale*, vol. 5, no. 9, pp. 3620–3626, 2013.

[8] D. Sarkar, W. Liu, X. Xie, A. C. Anselmo, S. Mitragotri, and K. Banerjee, "$MoS_2$ field-effect transistor for next-generation label-free biosensors," *ACS Nano*, vol. 8, no. 4, pp. 3992–4003, 2014.

[9] D. Sarkar and K. Banerjee, "Proposal for tunnel-field-effect-transistor as ultra-sensitive and label-free biosensors," *Applied Physics Letters*, vol. 100, no. 14, Article ID 143108, 2012.

[10] W. Bao, X. Cai, D. Kim, K. Sridhara, and M. S. Fuhrer, "High mobility ambipolar $MoS_2$ field-effect transistors: substrate and dielectric effects," *Applied Physics Letters*, vol. 102, no. 4, Article ID 042104, 2013.

[11] K. Kalantar-Zadeh, J. Z. Ou, T. Daeneke, M. S. Strano, M. Pumera, and S. L. Gras, "Two-dimensional transition metal dichalcogenides in biosystems," *Advanced Functional Materials*, vol. 25, no. 32, pp. 5086–5099, 2015.

[12] P. R. Nair and M. A. Alam, "Theory of "Selectivity" of label-free nanobiosensors: a geometro-physical perspective," *Journal of Applied Physics*, vol. 107, no. 6, Article ID 064701, 2010.

[13] P. R. Nair and M. A. Alam, "Performance limits of nanobiosensors," *Applied Physics Letters*, vol. 88, no. 23, Article ID 233120, 2006.

[14] G. Saltzgaber, P. Wojcik, T. Sharf et al., "Scalable graphene field-effect sensors for specific protein detection," *Nanotechnology*, vol. 24, no. 35, Article ID 355502, 2013.

[15] I. Meric, M. Y. Han, A. F. Young, B. Ozyilmaz, P. Kim, and K. L. Shepard, "Current saturation in zero-bandgap, top-gated graphene field-effect transistors," *Nature Nanotechnology*, vol. 3, no. 11, pp. 654–659, 2008.

[16] P. Sharma, V. Mangla, and R. Dhyani, "The zero band gap semiconductor: graphene," *International Journal of Innovative Research in Technology*, vol. 1, no. 6, 2014.

[17] S. D. Sarma, S. Adam, E. H. Hwang, and E. Rossi, "Electronic transport in two-dimensional graphene," *Reviews of Modern Physics*, vol. 83, no. 2, pp. 407–470, 2011.

[18] A. H. Castro Neto, F. Guinea, N. M. R. Peres, K. S. Novoselov, and A. K. Geim, "The electronic properties of graphene," *Reviews of Modern Physics*, vol. 81, no. 1, pp. 109–162, 2009.

[19] H. Karimi, M. T. Ahmadi, E. Khosrowabadi et al., "Analytical prediction of liquid-gated graphene nanoscroll biosensor performance," *RSC Advances*, vol. 4, no. 31, pp. 16153–16162, 2014.

[20] I. Meric, N. Baklitskaya, and P. Kim, "RF performance of top-gated, zero-bandgap graphene field-effect transistors," in *Proceedings of the IEEE International Electron Devices Meeting*, pp. 1–4, San Francisco, Calif, USA, December 2008.

[21] K. N. Parrish, M. E. Ramon, S. K. Banerjee, and D. Akinwade, "A compact model for graphene FETs for linear and non-linear circuits," in *Proceedings of the IEEE International Conference on Simulation of Semiconductor Processes and Devices (SISPAD '12)*, pp. 75–78, IEEE, Denver, Colo, USA, 2012.

[22] Y. Ohno, K. Maehashi, Y. Yamashiro, and K. Matsumoto, "Electrolyte-gated graphene field-effect transistors for detecting pH and protein adsorption," *Nano Letters*, vol. 9, no. 9, pp. 3318–3322, 2009.

[23] K. L. Shepard, I. Meric, and P. Kim, "Characterization and modeling of graphene field-effect devices," in *Proceedings of the International Conference on Computer-Aided Design (ICCAD '08)*, pp. 406–411, San Jose, Calif, USA, November 2008.

Journal of
Engineering

The Scientific
World Journal

International Journal of
Rotating
Machinery

Journal of
Sensors

International Journal of
Distributed
Sensor Networks

Advances in
Civil Engineering

Journal of
Control Science
and Engineering

Journal of
Robotics

Journal of
Electrical and Computer
Engineering

Hindawi

Submit your manuscripts at
http://www.hindawi.com

Advances in
OptoElectronics

VLSI Design

International Journal of
Navigation and
Observation

Modelling &
Simulation
in Engineering

International Journal of
Aerospace
Engineering

International Journal of
Chemical Engineering

International Journal of
Antennas and
Propagation

Active and Passive
Electronic Components

Shock and Vibration

Advances in
Acoustics and Vibration